PHYSICAL REVIEW B **70**, 100102(R) (2004)

Density-functional-theory-based local quasicontinuum method: Prediction of dislocation nucleation

Matt Fago,[1] Robin L. Hayes,[2] Emily A. Carter,[2] and Michael Ortiz[1]
[1]*Graduate Aeronautical Laboratories, California Institute of Technology, Pasadena, California 91125, USA*
[2]*Department of Chemistry and Biochemistry, University of California, Los Angeles, California 90025, USA*
(Received 2 June 2004; revised manuscript received 30 June 2004; published 27 September 2004)

We introduce the density functional theory (DFT) local quasicontinuum method: a first principles multiscale material model that embeds DFT unit cells at the subgrid level of a finite element computation. The method can predict the onset of dislocation nucleation in both single crystals and those with inclusions, although extension to lattice defects awaits new methods. We show that the use of DFT versus embedded-atom method empirical potentials results in different predictions of dislocation nucleation in nanoindented face-centered-cubic aluminum.

DOI: 10.1103/PhysRevB.70.100102 PACS number(s): 61.72.−y, 31.15.Ew, 02.70.−c, 46.15.−x

In this paper we establish the feasibility of embedding density functional theory (DFT) into large-scale macroscopic finite-element calculations. The embedding takes place at the subgrid level and exploits the Cauchy-Born hypothesis,[1] whereby the local deformation computed at a quadrature point of the finite-element grid is applied to an infinite crystal lattice, whose energy and state of stress is then evaluated with DFT. We call our method DFT-LQC in reference to the local quasicontinuum (LQC) or Cauchy-Born approach,[2] in anticipation of a future nonlocal extension of the method.

The impetus for multiscale descriptions of materials such as DFT-LQC derives from two main sources. From a top-down viewpoint, empirical constitutive models which remain reliable under extreme conditions of pressure, deformation, and deformation rate are often not available for use in large-scale engineering simulations. Alternately, it is often desirable to extend the applicability of fundamental theories to engineering spatial and temporal scales. Methods such as DFT-LQC meet these demands by supplying a fundamental description of the material and embedding this description into large-scale engineering simulations.

The LQC method, including extensions dealing with complex lattices, has been extensively used by Tadmor *et al.*,[3,4] who used the method to study the nanoindentation of silicon and to analyze the process of polarization switching in $PbTiO_3$. Tadmor *et al.* based their subgrid atomistic calculations on empirical potentials or effective Hamiltonians fitted to first principles calculations.

The chief contribution of the present work is to establish the feasibility of using DFT, as opposed to empirical or effective interatomic potentials, as the fundamental description of materials such as aluminum in LQC calculations. Since DFT is a first-principles theory (see Ref. 5, and references therein for background), it may be expected to result in increased fidelity of the calculations, especially when the material is subject to an environment where the empirical potentials were not calibrated. A case in point is provided by nanoindentation, which induces high pressures and deformations under the indenter, even in the elastic range. Indeed, we show that the use of DFT versus embedded-atom method (EAM) empirical potentials results in vastly different predictions of dislocation nucleation in nanoindented face-centered-cubic (fcc) aluminum.

The general DFT-LQC method consists of embedding DFT calculations at the integration points of the finite element mesh. Specifically, the energy density $W(\mathbf{F})$ and stresses

$$P_{iJ} = \frac{\partial W}{\partial F_{iJ}} \tag{1}$$

at each quadrature point are obtained by applying the local deformation gradient $\mathbf{F}$ uniformly to a properly oriented crystallographic unit cell. In view of the periodic boundary conditions applied to each unit cell, this approach idealizes the material in the vicinity of an integration point as a perfect infinite crystal undergoing the specified uniform deformation. While local electronic effects are accounted for in this manner, the unit cells interact only through the macroscopic elastic field.

The ground state of each unit cell follows from the stationarity principle

$$\frac{\partial E^{\mathrm{Tot}}[\rho(\mathbf{r});\mathbf{F}]}{\partial \rho(\mathbf{r})} = \frac{\partial E^{\mathrm{Hart}}[\rho(\mathbf{r});\mathbf{F}]}{\partial \rho(\mathbf{r})} + \frac{\partial E^{\mathrm{xc}}[\rho(\mathbf{r});\mathbf{F}]}{\partial \rho(\mathbf{r})} + \frac{\partial T_s[\rho(\mathbf{r});\mathbf{F}]}{\partial \rho(\mathbf{r})} + V_{Ext}[\mathbf{r};\mathbf{F}] = \mu, \tag{2}$$

where $\rho(r)$ is the local electron density, $E^{\mathrm{Hart}}[\rho(\mathbf{r});\mathbf{F}]$ is the electron-electron Coulomb repulsion energy, $E^{\mathrm{xc}}[\rho(\mathbf{r});\mathbf{F}]$ is the exchange-correlation energy, $T_s[\rho(\mathbf{r});\mathbf{F}]$ is the electronic kinetic energy, $V_{Ext}[\mathbf{r};\mathbf{F}]$ is the ionic potential, and μ is the chemical potential. The energy and stress from the DFT calculations, once normalized by the volume of the unit cell to obtain $W(\mathbf{F})$, are provided to the finite element solver, which then determines the system's equilibrium state via energy minimization.

In traditional DFT implementations[6] the density is expanded into orbitals, which has the advantage of providing an exact expression for the (noninteracting) electron kinetic energy, but it comes at a cost, namely, the orthogonalization of the orbitals. Since orthogonalization is an $O(N^3)$ opera-

tion, large calculations become expensive. Furthermore, orbitals require *k*-point sampling,[5] which often increases the computational cost by a factor of 1000 for metals.

If instead the variational problem Eq. (2) is solved directly with the electron density,[7] the orthogonalization and *k*-point sampling are eliminated. This results in an $O[N\ln(N)]$ algorithm that is 2–5 orders of magnitude less costly than orbital-based methods of similar accuracy, even for a primitive unit cell.[8] Unfortunately, the exact form of the kinetic energy functional is unknown. Nonetheless, orbital-free density functional theory (OFDFT) has proven to be reliable for simple metallic systems using a linear-response-based kinetic energy functional.[8] It is the use of the efficient OFDFT that renders DFT–LQC viable in terms of cost.

As an example application of the method, we study the nucleation of dislocations during nanoindentation of fcc aluminum (see Refs. 9–11, and references therein for background). In this application, the nucleation of the first dislocation signals the end of the elastic range and the onset of plasticity. Since the process of homogeneous nucleation of a dislocation requires stresses of the order of the theoretical strength of the crystal, and involves large distortions of the lattice, the use of empirical potentials under such conditions may lead to unreliable results. Unfortunately, *in situ* identification of the spatial location and character of the first dislocation is not possible,[12,13] which precludes direct comparison with experiment. Although experimental load-displacement results are readily available,[14] the current method only yields the characteristics of the initial dislocation in a perfect crystal, rather than predicting the full plastic behavior involving many dislocations. However, our analysis clearly demonstrates that DFT- and EAM-based calculations lead to sharply different dislocation emission results.

Following Refs. 11 and 15, we view dislocation nucleation as a local instability of the crystal lattice. Specifically, we identify the onset of instability as the loss of the local ellipticity of the equations governing the incremental equilibrium of the crystal.[16,17] Let **F** be the local deformation at a point of a deforming solid, $W(\mathbf{F})$ the corresponding strain-energy density, and

$$C_{iJkL} = \frac{\partial P_{iJ}}{\partial F_{kL}} = \frac{\partial W}{\partial F_{iJ}\partial F_{kL}} \tag{3}$$

the tangent moduli. The incremental equations of equilibrium of a solid are elliptic at a point if

$$C_{iJkL}N_J N_L k_i k_k = A_{ik}(\mathbf{N})k_i k_k > 0 \tag{4}$$

for all vectors **N** and **k**. Here

$$A_{ik}(\mathbf{N}) = C_{iJkL}N_J N_L \tag{5}$$

is the acoustic tensor of the deformed crystal. When condition (4) is satisfied everywhere in the solid, the incremental displacement solution is unique and the behavior of the solid is deemed stable. Ellipticity is lost when vectors **N** and **k** can be found such that

$$\Lambda = C_{iJkL}N_J N_L k_i k_k = A_{ik}(\mathbf{N})k_i k_k \leqslant 0. \tag{6}$$

As noted by Suresh *et al.*,[15] the vector **N** then defines the emerging characteristic direction and **k** is the corresponding polarization vector. The angle between **N** and **k** affords a first classification of the local unstable modes. Thus, if **k** is orthogonal to **N** the local unstable mode is one of shear, and the point of instability may be identified with the onset of dislocation nucleation.

Since the energy density $W(\mathbf{F})$ and the stress tensor $\mathbf{P}(\mathbf{F})$ are computed from DFT at all quadrature points, the tangent moduli $\mathbf{C}(\mathbf{F})$ are also readily available by numerical differentiation of $\mathbf{P}(\mathbf{F})$. It is therefore a straightforward matter to verify the stability condition (6). Leroy and Ortiz,[18] and Van Vliet *et al.*,[15] perform this calculation in general terms by minimizing the eigenvalues of the acoustic tensor (5), with a zero eigenvalue signaling the onset of instability. For simplicity, we explicitly identify the potentially unstable directions **N** with the known slip systems of a fcc crystal. Thus, the positive definiteness of the acoustic tensor is verified for each of the $\{111\}$ family of slip planes and the $\langle 110\rangle$ and $\langle 112\rangle$ family of slip directions, corresponding to the perfect and partial fcc slip systems, respectively. The minimum of these 24 scalar values represents the stability of the given unit cell, with a nonpositive value indicating nucleation of the corresponding dislocation.

Indentation is examined on both the (111) and $(\bar{1}\bar{1}0)$ surfaces. The bulk solid is represented by a $2\ \mu\text{m}\times 1\ \mu\text{m}\times 1\ \mu\text{m}$ mesh using 210 ten-node large strain tetrahedral elements with four quadrature points. The exterior boundary of the solid was fixed, with a mirror plane to exploit the symmetry of the slip system. The sample was indented with a hard[10] 750 nm spherical indenter until the formation of the first dislocation, after which the calculation was stopped.

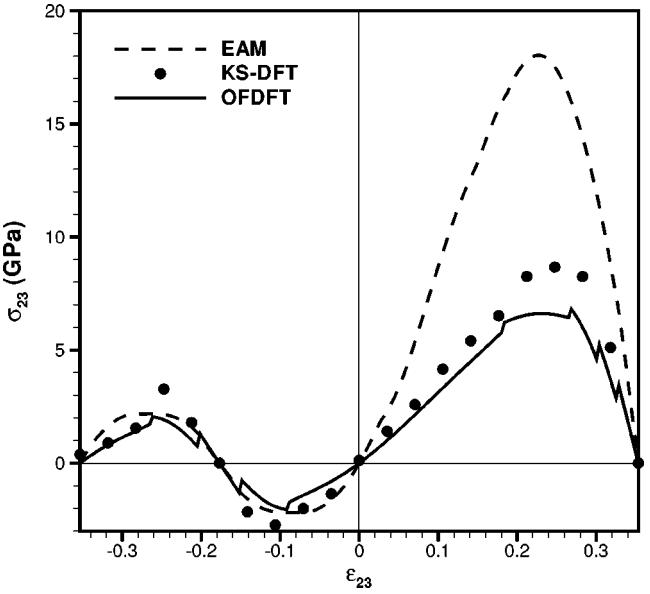

FIG. 1. Resolved shear stress-strain curves along the $[\bar{1}\bar{1}2]$ direction using EAM, OFDFT, and Kohn-Sham (KS) DFT models of fcc aluminum.

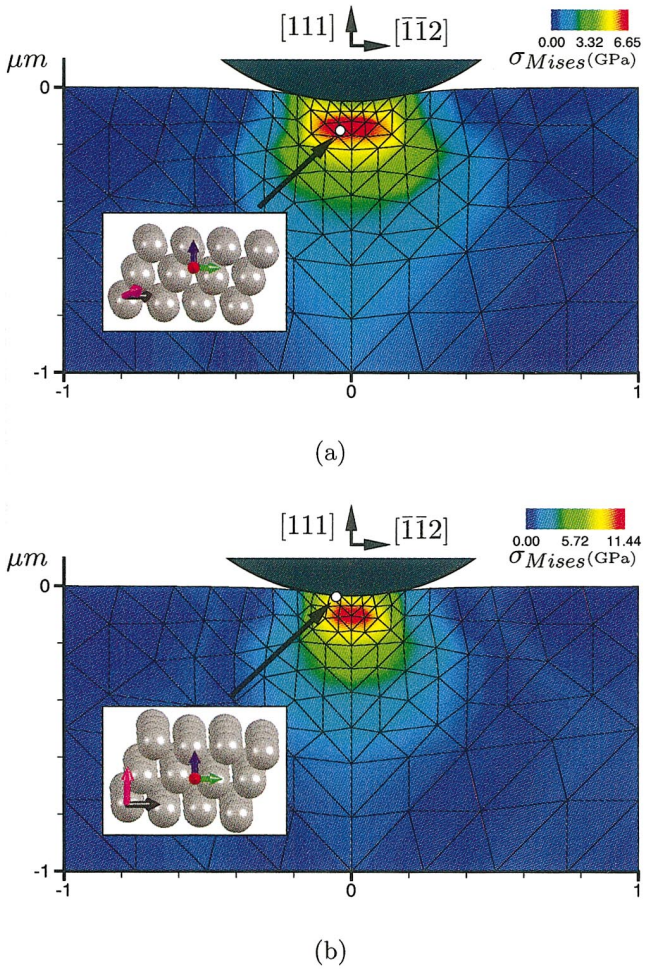

FIG. 2. (Color) Deformed mesh, von Mises stresses, and dislocation results at initial instability for (111) indentation. The DFT result (a) is at 50 nm indentation, while the EAM result (b) is indented 35 nm. The circles indicate incipient dislocations, with the deformed lattice for the most unstable dislocation shown in the inset. The magenta and grey arrows indicate the computed slip plane normal and Burgers vectors, respectively. Note the differences in the stress scales in (a) and (b).

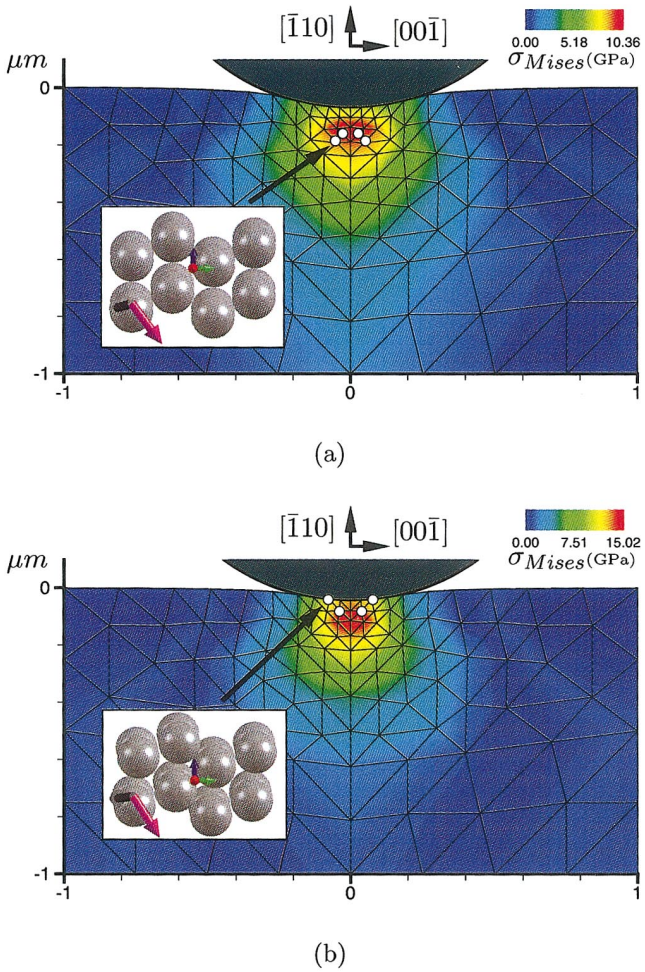

FIG. 3. (Color) Deformed mesh, von Mises stresses, and dislocation results at initial instability for $(\bar{1}10)$ indentation using (a), DFT and (b) EAM-based constitutive models. The DFT result (a) is at 70 nm indentation, while the EAM result (b) is indented 45 nm. The circles indicate incipient dislocations, with the deformed lattice for the most unstable dislocation shown in the inset. The magenta and grey arrows indicate the computed slip plane normal and Burgers vectors, respectively. Note the differences in the stress scales in (a) and (b).

Note that this indenter size is well outside the range accessible to molecular dynamics simulations, ≈10 nm.

The OFDFT calculations[8] employed the commonly used Goodwin local pseudopotential,[19] the local density approximation (LDA) exchange and correlation, the Wang-Teter density-independent linear response kinetic energy functional, a kinetic energy cutoff of 60 Ry, and a primitive unit cell. The EAM calculations, similarly performed at the subgrid level, utilized the code made available to the public by Miller and Tadmor[20] which implements the Ercolessi and Adams[21] potential.

Note that OFDFT, as described, underestimates the elastic constants near the equilibrium position, although the lattice spacing and bulk modulus are well-reproduced. EAM Al agrees with the experimental elastic constants better as it was explicitly fit to the Kohn-Sham DFT LDA elastic constants, which fortuitously more closely match the experimental values, but there is no reason to expect that it will capture the correct physical behavior under highly deformed configurations. Indeed, it is known that EAM Al potentials do not accurately model the unstable stacking fault energy, while DFT is offered as a better approach.[22] While the shear response of the OFDFT compares well to that obtained with a Kohn-Sham DFT formulation with similar parameters and the same local pseudopotential, Fig. 1, the results differ significantly from those obtained with the EAM. Likewise, the unstable stacking fault energies, without allowing the ions to relax, are 85, 93, and 130 mJ/m^2 for the OFDFT, KSDFT, and EAM[22] methods, respectively. Although the EAM value more closely agrees with other calculated values, the close agreement between OFDFT and KSDFT suggest that the unstable stacking fault energy could be improved with a better local pseudopotential.

Examining the initial dislocation structures obtained for the (111) orientation, Fig. 2, it is apparent that the two con-

stitutive relations result in qualitatively different behavior. While both models indicate nucleation of $[0\bar{1}1]$ dislocations, the OFDFT model predicts a single dislocation will form in the $(\bar{1}11)$ slip plane at 50 nm indentation at a load of 980 μN, off axis, and at 0.15 μm below the surface and 0.10 μm from the indenter surface, Fig. 2(a). The response for the EAM model, shown in Fig. 2(b), indicates one dislocation unexpectedly forms in the (111) slip plane after 35 nm indentation at a load of 1040 μN, off axis, 0.04 μm below the surface, and 0.01 μm from the indenter surface. For the deformation indicated to be unstable by OFDFT using Eq. (6), $\Lambda=0$ GPa, the EAM computes an unstable value of -4 GPa.

For the $(\bar{1}10)$ orientation, DFT predicts two matching sets of $\langle 112\rangle$ partials near the location of the maximum von Mises stress, Fig. 3(a), which form a $[00\bar{1}]$ dislocation. By contrast, the EAM model produces four partial dislocations closer to the surface, with the maximum stress again much closer to the surface. Of particular note is the significant difference in indentation depth required for nucleation: 70 nm for DFT versus 45 nm for the EAM, corresponding to loads of 1800 and 1460 μN, respectively. The larger load required to nucleate the first dislocation when indenting the $\mathrm{Al}(\bar{1}10)$ surface compared to the Al(111) surface agrees with experiment.[23] For the deformations indicated to be unstable by OFDFT, $\Lambda=0$ to -1 GPa, while with the EAM, $\Lambda=+4$ to $+5$ GPa. The first dislocations obtained with both the EAM and DFT-LQC lie within the upper bound provided by the elastic-plastic boundary obtained experimentally for Al(100) via atomic force microscopy.[14]

In closing, some of the limitations and possible extensions of the method are noteworthy. The Cauchy-Born rule, as used in the present implementation of the method, does not permit the description of lattice defects such as dislocations. This limitation could be overcome with the full quasicontinuum method where the finite element mesh can be resolved down to individual atoms. However, this awaits the development of a fast, nonperiodic DFT code that can embed atomic clusters into a deformed crystal. Although local pseudopotentials[24] and kinetic energy functionals are an active area of research,[25] currently only metallic systems are well described by OFDFT, limiting the types of materials that can be addressed with this method.

Despite these limitations, the examples presented establish the feasibility of embedding the DFT calculations at the subgrid level in finite-element calculations. The sharp differences between the DFT and EAM predictions of dislocation nucleation in calculations of nanoindentation of aluminum calls the reliability of the latter into question, and suggests the need for the more fundamental description of material behavior afforded by DFT.

The authors are grateful to the U.S. Department of Defense for support provided through Brown University's MURI Center for the "Design and Testing of Materials by Computation: A Multi-Scale Approach," to the DOE through Caltech's ASCI/ASAP Center for the Simulation of the Dynamic Response of Solids, and for the EAM code provided by Ron Miller and Ellad B. Tadmor (see Ref. 20). M.F. thanks the CSGF for support. R.L.H. thanks NDSEGF for funding.

[1] M. Born, Proc. Cambridge Philos. Soc. **36**, 160 (1940).
[2] E. Tadmor, M. Ortiz, and R. Phillips, Philos. Mag. A **73**, 1529 (1996).
[3] G. Smith, E. Tadmor, N. Bernstein, and E. Kaxiras, Acta Mater. **49**, 4089 (2001).
[4] E. Tadmor, U. Waghmare, G. Smith, and E. Kaxiras, Acta Mater. **50**, 2989 (2002).
[5] M. Payne, M. Teter, D. Allan, T. Arias, and J. Joannopoulos, Rev. Mod. Phys. **64**, 1045 (1992).
[6] W. Kohn and L. Sham, Phys. Rev. **140**, A1133 (1965).
[7] P. Hohenberg and W. Kohn, Phys. Rev. **136**, B864 (1964).
[8] S. Watson and E. Carter, Comput. Phys. Commun. **128**, 67 (2000).
[9] E. Tadmor, R. Miller, R. Phillips, and M. Ortiz, J. Mater. Res. **14**, 2233 (1999).
[10] J. Knap and M. Ortiz, Phys. Rev. Lett. **90**, 226102 (2003).
[11] J. Li, K. Van Vliet, T. Zhu, S. Yip, and S. Suresh, Nature (London) **418**, 307 (2002).
[12] S. Corcoran, R. Colton, E. Lileodden, and W. Gerberich, Phys. Rev. B **55**, R16 057 (1997).
[13] W. Gerberich, J. Nelson, E. Lilleodden, P. Anderson, and J. Wyrobek, Acta Mater. **44**, 3585 (1996).
[14] N. Tymiak, D. Kramer, D. Bahr, T. Wyrobek, and W. Gerberich, Acta Mater. **49**, 1021 (2001).
[15] K. Van Vliet, J. Li, T. Zhu, S. Yip, and S. Suresh, Phys. Rev. B **67**, 104105 (2003).
[16] R. Hill, J. Mech. Phys. Solids **10**, 1 (1962).
[17] J. Rice, in *Proceedings of the 14th International Congress on Theoretical and Applied Mechanics*, edited by W. L. Koiter (North-Holland, Amsterdam, 1976), p. 207.
[18] Y. Leroy and M. Ortiz, Int. J. Numer. Analyt. Meth. Geomech. **13**, 53 (1989).
[19] L. Goodwin, R. Needs, and V. Heine, J. Phys.: Condens. Matter **2**, 351 (1990).
[20] R. Miller and E. Tadmor, *Quasicontinuum Method Website*, http://www.qcmethod.com
[21] F. Ercolessi and J. Adams, Europhys. Lett. **26**, 583 (1994).
[22] J. Zimmerman, H. Gao, and F. Abraham, Modell. Simul. Mater. Sci. Eng. **8**, 103 (2000).
[23] A. Gouldstone, H. Koh, K. Zeng, A. Giannakopoulos, and S. Suresh, Acta Mater. **48**, 2277 (2000).
[24] B. Zhou, Y. Wang, and E. Carter, Phys. Rev. B **69**, 155329 (2004).
[25] Y. Wang and E. Carter, in *Theoretical Methods in Condensed Phase Chemistry*, Progress in Theoretical Chemistry and Physics, edited by S. Schwartz (Kluwer, Dordrecht, 2000), pp. 117–184.